

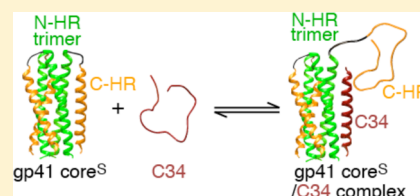
The C34 Peptide Fusion Inhibitor Binds to the Six-Helix Bundle Core Domain of HIV-1 gp41 by Displacement of the C-Terminal Helical Repeat Region

John M. Louis,* James L. Baber, and G. Marius Clore*

Laboratory of Chemical Physics, National Institute of Diabetes and Digestive and Kidney Diseases, National Institutes of Health, Bethesda, Maryland 20892-0520, United States

S Supporting Information

ABSTRACT: The conformational transition of the core domain of HIV-1 gp41 from a prehairpin intermediate to a six-helix bundle is responsible for virus–cell fusion. Several inhibitors which target the N-heptad repeat helical coiled-coil trimer that is fully accessible in the prehairpin intermediate have been designed. One such inhibitor is the peptide C34 derived from the C-heptad repeat of gp41 that forms the exterior of the six-helix bundle. Here, using a variety of biophysical techniques, including dye tagging, size-exclusion chromatography combined with multiangle light scattering, double electron–electron resonance EPR spectroscopy, and circular dichroism, we investigate the binding of C34 to two six-helix bundle mimetics comprising N- and C-heptad repeats either without (core^{SP}) or with (core^{S}) a short spacer connecting the two. In the case of core^{SP} , C34 directly exchanges with the C-heptad repeat. For core^{S} , up to two molecules of C34 bind the six-helix bundle via displacement of the C-heptad repeat. These results suggest that fusion inhibitors such as C34 can target a continuum of transitioning conformational states from the prehairpin intermediate to the six-helix bundle prior to the occurrence of irreversible fusion of viral and target cell membranes.



The entry of HIV-1 into target cells is mediated by the surface envelope (Env) glycoproteins gp120 and gp41.¹ The initial event involves binding of CD4 and the chemokine coreceptor on the target cell to gp120 on the surface of the virus, followed by a series of conformational changes in gp120 and gp41 that ultimately result in fusion of the viral and cell membranes.^{2–7} Early steps in this process have been visualized by crystallography and cryo-electron microscopy of a cleaved HIV-1 Env trimer, thought to represent an activated state of gp120 or gp41.^{8,9} The gp41 component in these structures is in a prefusion state, approximating the prehairpin intermediate,^{4,10–12} in which the trimeric coiled-coil N-heptad repeat (N-HR, residues 543–582) and the C-terminal heptad repeat (C-HR, residues 625–662) do not interact with one another, and the C- and N-termini of gp41 bridge the viral and target cell membranes, respectively. Further conformational changes in gp41 result in the formation of a six-helix bundle in which the N-HR trimeric helical coiled coil is surrounded by three C-HR helices packed as antiparallel helices into hydrophobic grooves,^{13–16} thereby bringing the viral and target cell membranes into direct contact with one another.^{4,17,18}

Previous work showed that HIV-1 fusion can be blocked by targeting the N-HR and C-HR in the prehairpin intermediate.^{10,19–26} Inhibitors directed against the trimeric N-HR helical coiled-coil²⁷ include peptides derived from the C-HR^{10,19} (such as C34 and T20) and antibodies that directly bind to the N-HR trimer,^{22,28–41} as well as a peptide [N36^{Mut(e,g)}] derived from the N-HR that sequesters the N-HR of gp41 into inactive heterotrimers.^{42,43} The temporal window for inhibitors directed

against the N-HR trimer of gp41 is similar with a half-life of 20–25 min post-CD4 engagement.^{31,43}

In the series of monoclonal antibodies generated in our laboratory by selection against N-HR trimer mimetics,^{29–33} we made the interesting discovery that these antibodies not only bound prehairpin intermediate mimetics in which two or more N-HR helices of the trimer are fully exposed, but also bound directly to six-helix bundle mimetics.⁴⁴ Further, neutralization activity was far better correlated to affinity for the six-helix bundle than for the prehairpin intermediate.⁴⁴ Unexpectedly, binding of these neutralizing antibodies to the six-helix bundle did not occur via displacement of the C-HR helices, as might have been predicted on the basis of crystal structures with prehairpin intermediate mimetics,^{32,33} but was mapped to an epitope formed by a relatively small hydrophobic pocket on the N-HR that is exposed in the context of the six-helix bundle.⁴⁴ The equilibrium dissociation constants (K_{diss}) for binding of C34 to a prehairpin mimetic 5-helix, a single-chain construct lacking the last C-HR helix, as well as for six-helix bundle formation upon mixing N-HR and C-HR peptides, range from 0.3 to 2 μM , as determined by isothermal titration calorimetry.^{45–47} Thus, there appears to be a discrepancy between K_{diss} values for the binding of C34 to prehairpin intermediate mimetics *in vitro* and IC_{50} values ranging from 4 to 70 nM, depending upon HIV-1 strain, for inhibition of HIV-1 fusion in cell-based assays.^{17,48} Here we investigate the

Received: September 15, 2015

Revised: October 27, 2015

Published: October 27, 2015

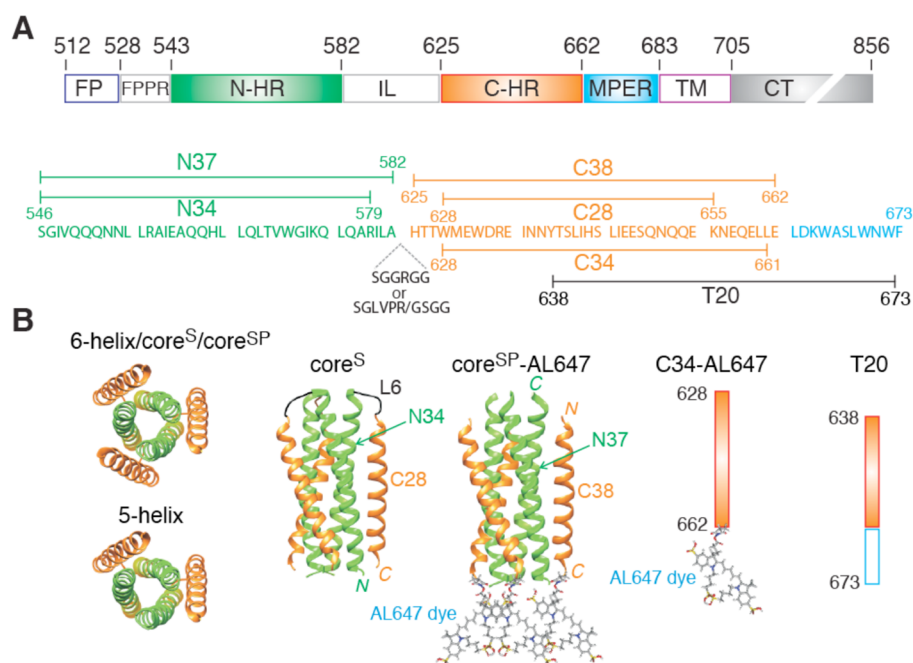


Figure 1. Domain organization and gp41 constructs used in this work. (A) Domain organization of HIV-1 gp41. Abbreviations: FP, fusion peptide; FPPR, fusion peptide proximal region; N-HR, N-heptad repeat; IL, immune-dominant linker; C-HR, C-heptad repeat; MPER, membrane proximal external region; TM, transmembrane region; CT, intraviral C-terminal domain. The numbering of residues corresponds to their positions in the HIV-1 Env sequence. (B) Constructs used in this work. The coordinates of the six-helix bundle formed by an internal trimer of N-HR helical repeats surrounded by three C-HR helical repeats are taken from ref 16 (Protein Data Bank entry 1SZT). 6-helix and 5-helix are single-chain constructs differing by the presence and absence, respectively, of the C-terminal C-HR helix. Core^S is a homotrimer in which the N-HR and C-HR helices of each subunit are connected by a six-residue linker (SGGRGG). In the core^{SP} six-helix bundle construct, the N-HR and C-HR helices are not connected by a linker. Sites of labeling of core^{SP} and the C34 peptide with the Alexafluor 647 dye (AL647) are indicated.

interaction of C-HR-derived peptide C34 with two six-helix bundle domain constructs of gp41 differing in whether the N-HR and C-HR regions are covalently linked to one another and show that, in contrast to the case for N-HR-directed monoclonal antibodies, binding occurs in both instances via direct displacement of the C-HR helices. We show that in the case of the six-helix bundle construct in which the N-HR is linked to the C-HR by a six-residue spacer sequence (core^S), instead of the full-length, 42-residue, immune-dominant linker (IL) sequence, only two of the three C-HR helices are displaced by C34 with a K_{diss} of $\sim 1 \mu\text{M}$.

MATERIALS AND METHODS

gp41 Constructs. The gp41 analogues used in this study are depicted schematically in Figure 1 and comprise a single-chain six-helix bundle (6-helix),²¹ a single-chain five-helix bundle (5-helix),²¹ core^S,¹⁶ core^{SP},⁴⁴ C34,¹³ and T20.¹⁹ DNA inserts were cloned in pET11a or pET15 vectors between NdeI/BamHI and NcoI/BamHI sites, respectively. To facilitate the isolation of recombinant C34-Cys (628–662) bearing the E662C substitution, a modified core^S construct (N37-SGLV-PRGS-C34) was created by exchanging the L6 spacer sequence to encompass a thrombin site between the N-HR (N37) and C-HR (C34) regions. Core^{SP}-Cys, which bears the same C-terminal E662C substitution as C34-Cys, was engineered from the core^{SP} template⁴⁴ by QuikChange mutagenesis (Agilent Technologies, Santa Clara, CA). DNA sequences were verified by sequencing. T20 was obtained from the NIH Reference Reagent Program. Chemically synthesized C34 (Ac-C-HR^{628–661}-NH₂) was purchased from Commonwealth Biotechnologies, Inc. (Richmond, VA).

Protein Purification, Folding, and Labeling with Alexafluor 647 Dye.

Escherichia coli BL21(DE3) bearing the appropriate plasmid was grown in Luria-Bertani medium and induced for expression at an A_{600} of 0.7 for 4 h. All expressed gp41 constructs invariably accumulate in the insoluble fraction. After isolating the insoluble fraction, the constructs were fractionated on size-exclusion Superdex-200 or -75 columns (GE Healthcare, Piscataway, NJ) under denaturing conditions followed by reverse-phase high-performance liquid chromatography as described previously.⁴⁹ 6-helix, 5-helix, core^S, and core^{SP} were folded by dialysis against 50 mM sodium formate (pH 3) followed by buffer exchange with 10 mM Tris-HCl (pH 7.6) and 150 mM NaCl (buffer A), concentrated to $\sim 2 \text{ mg/mL}$, and stored.

Core^{SP}-Cys was subjected to fractionation on a Superdex-75 column in buffer A containing 2 mM tris(2-carboxyethyl)-phosphine hydrochloride (TCEP) (Sigma) to keep the cysteine residues reduced. Peak fractions were pooled, concentrated, and stored at $-20 \text{ }^\circ\text{C}$ prior to labeling. An aliquot of core^{SP}-Cys was reacted with a 2–3-fold molar excess of Alexafluor 647 (AL647) C₂-maleimide (Life Technologies) for $\sim 2.5 \text{ h}$. The reaction was terminated by the addition of 2-mercaptoethanol (Sigma) to a final concentration of 10 mM, and the mixture was incubated for 10 min, followed by fractionation on a Superdex-75 column in buffer A to remove the unreacted dye. Peak fractions corresponding to core^{SP}-AL647 were pooled, concentrated, and stored. Recombinant C34-Cys was labeled with excess AL647 C₂-maleimide in 6 M guanidine hydrochloride and 25 mM Tris-HCl at pH 8 for 2.5 h, purified on a Superdex-30 column to remove excess dye followed by anion-

exchange (mono Q 5/50 GL, GE Healthcare) chromatography to remove the unlabeled C34-Cys, concentrated, and stored.

Theoretical masses of the proteins used are as follows: 6-helix, 29470 Da; 5-helix, 24459 Da; core^S, 8284 Da (per subunit); core^{SP}, 5216 Da for the N-HR (GSHM-N37-SGLVPR) and 4975 Da for the C-HR (GSGG-C38); recombinant C34-Cys, 4610 Da; synthetic C34, 4290 Da; and T20, 4492 Da. Recombinant C34-Cys contains four non-native residues, GSGG, at the N-terminus. The composition of purified proteins and the extent of AL647 labeling were verified by electrospray ionization mass spectrometry (ESI-MS). All experiments were conducted in 10 mM Tris-HCl (pH 7.6) and 150 mM NaCl (buffer A) at room temperature unless stated otherwise.

Native Polyacrylamide Gel Electrophoresis (native-PAGE), Size-Exclusion Chromatography (SEC), and SEC with Multiangle Light Scattering (SEC-MALS). Samples were mixed to give a final concentration of 10 μM core^S or core^{SP} trimer and an increasing molar ratio from 1- to 10-fold for C34 or T20 as indicated below the gel panels. Following incubation for 30 min at room temperature, the samples were subjected to electrophoresis on 20% homogeneous PhastGels (GE Healthcare) using 4 μL for each six-lane applicator and native buffer strips. Gels were stained in PhastGel Blue R, destained, and digitized.

Samples for evaluating the displacement of C38-AL647 from core^{SP}-AL647 and concomitant binding of C34 were mixed to a final volume of 100 μL /injection, and incubated for at least 30 min, followed by application to a Superdex-75 column pre-equilibrated and run in buffer A at a flow rate of 0.5 mL/min.

Molecular masses were estimated by analytical SEC with in-line MALS (DAWN Heleos-II, Wyatt Technology Inc., Santa Barbara, CA), refractive index (Optilab T-rEX, Wyatt Technology Inc.), and UV (Waters 2487, Waters Corp., Milford, MA) detectors. Typically, the protein (150–200 μg in 100 μL) either by itself or mixed with a 5-fold molar excess of C34 was applied to a pre-equilibrated Superdex-75 column (1.0 cm \times 30 cm, GE Healthcare) and eluted at a flow rate of 0.5 mL/min in buffer A. Samples when mixed with C34 peptide were incubated for at least 30 min prior to injection. Molecular masses were calculated using Astra version 6.1 provided with the instrument.

Circular Dichroism. CD spectra were recorded in buffer A at 20 °C on a JASCO J-810 spectropolarimeter using Spectra Manager software and a 0.1 cm path-length flat cell. Scans of core^S and core^{SP} were taken in the absence and presence of a 5-fold molar excess of C34. The α -helical content was determined using CDNN.⁵⁰

Defining a Method for Estimating the Binding Affinity of C34 for the gp41 Six-Helix Bundle. SEC coupled with monitoring of the distribution of the AL647 specific absorbance at 609 and 650 nm and protein absorbance at 280 nm was used to quantify the interaction of C34 with core^S and core^{SP}. The absorption spectrum of AL647 (and specifically the ratio of absorbance at 609 to 650 nm) is responsive to the intermolecular proximity of dye molecules (see Figure S1A). As association of two or more C34-AL647 peptides with core^S or core^{SP} results in a decrease in the absorbance at 650 nm and a corresponding increase at 609 nm, we used the sum of the two absorbance values to measure the total C34-AL647 eluting in each peak. Figure S1B shows the dependence of this sum with an increasing level of C34-AL647 with each injection. The total absorbance (for unbound C34-AL647 and its 1:1 and 1:2

complexes) matches the absorbance predicted for the amount of C34-AL647 added in each injection and thus validates the SEC/spectroscopic method used for quantitation.

C34-AL647 (1.4–33.8 μM) was titrated against a constant core^S trimer concentration of 2.33 μM in a total reaction/injection volume of 100 μL . After mixing, samples were equilibrated for more than 1 h prior to injection onto a Superdex-75 column (1 cm \times 30 cm) equilibrated and run in buffer A at a flow rate of 0.7 mL/min. Areas for C34-AL647, free and bound to core^S, were determined by integration of the peaks monitored at 280, 609, and 650 nm using PeakFit version 4.12 (Systat Software Inc., San Jose, CA). The area measured at 280 nm and the sum of areas measured at 609 and 650 nm were used for subsequent calculations. Fitting of the experimental titration data to the relevant equilibrium binding models was conducted numerically using the program FACSIMILE.⁵¹

DEER Analysis. Cysteine residues were introduced at the N- and C-termini of core^S (constructs termed N-Cys and C-Cys, respectively) by QuikChange mutagenesis. Deuteration and MTSL labeling of these two constructs were conducted as described previously⁵² and verified by ESI-MS. Data were collected on 50 μM (in subunits) N-Cys or C-Cys core^S samples in 10 mM Tris-HCl (pH 7.6) and 150 mM NaCl (buffer A) dissolved in a 30:70 mixture of *d*₈-glycerol and 99.99% D₂O in the absence or presence of a 1.2-fold molar excess (per core^S subunit) of C34. All DEER⁵³ data were collected at Q-band (33.8 GHz) on a Bruker E-580 spectrometer equipped with a 150 W traveling wave tube amplifier and a model ER5107D2 resonator. All experiments employed 8 ns pump (ELDOR) π pulses, 12 ns $\pi/2$ and 24 ns π observe pulses, a 95 MHz frequency difference between pump and observe pulses, and a 3.0 ms shot repetition time. The pump frequency was centered at the field spectrum maximum. The 400 ns half-echo periods of the first echo were incremented eight times in 16 ns increments to average ²H modulation. The pump pulse was incremented in 16 ns steps for the C34-bound C-Cys core^S sample. All other experiments utilized 8 ns pump pulse increments. All data were collected at 50 K. Samples were placed in 1.1 mm internal diameter quartz tubes (Wilma WG-221T-RB) and flash-frozen in liquid N₂. Total data collection times varied from ~3 to ~19 h. A 30–34 ns window was used for echo integration. On the basis of additional data collected for an experiment employing a shorter second echo period (not shown), data collected during the last 3 μs of the second echo period were deemed to be distorted for the C34-bound C-Cys core^S sample, possibly because of a “2 + 1” echo that results from excitation overlap of the pump and observe pulses. Therefore, data collected 3 μs prior to the end of the second echo period were not fitted for the C34-bound C-Cys core^S sample as indicated in Figure 5B. *P*(*r*) curves shown in Figure 5 were generated by Tikhonov Regularization in DeerAnalysis2013.⁵⁴ Ghost Suppression⁵⁵ for three spins was utilized in all fits. The regularization parameter, α , was determined by examination of the relevant L-curves ($\alpha = 10$ in all cases). A dimension of 3.0 was used for all exponential background corrections.

RESULTS AND DISCUSSION

Definition of Constructs and Peptides. Three constructs derived from the ectodomain of gp41 (Figure 1A), 6-helix, core^S, and core^{SP}, assemble to form a six-helix bundle (Figure 1B) that represents the fusogenic/postfusogenic state of gp41.

The single-chain six-helix construct consists of three tandem repeats of the N-HR^{543–582}-(L5)-C-HR^{625–662} segment connected by the five-residue spacer GSSGG; the L5 five-residue spacer (GGSGG) connects the N-HR and C-HR domains instead of the native immune-dominant linker (IL) domain of gp41. 5-helix is a truncated variant of 6-helix without the last C-terminal C-HR region and represents a prehairpin mimetic in which two neighboring N-HR helices are exposed. Core^S is a native six-helix bundle model comprising a trimer of three polypeptide chains, each bearing the arrangement N34^{546–579}-(L6)-C28^{628–655} (Figure 1); L6 is a six-residue spacer (SGGRGG). Core^{SP} is composed of six peptides, three each of N36^{546–582} and C38^{625–662}. Both core^S and core^{SP} are highly thermostable with melting temperatures of 80 and 68 °C, respectively (Figure S2). Peptides C34 and T20 span residues 628–661 and 638–673, respectively, of gp41. Core^{SP} bearing Alexafluor 647 dyes at the three C-termini of C38^{625–662} is termed core^{SP}-AL647, and C34 with the AL647 dye at its C-terminus is termed C34-AL647.

Binding of C34 to Single-Chain Six-Helix and Five-Helix Constructs. All experiments were conducted under nearly physiological conditions in 10 mM Tris-HCl buffer (pH 7.6) and 150 mM NaCl, ideal for stable trimerization of gp41,⁵⁶ as well as for direct comparison with our earlier binding studies of bivalent and single-chain antibodies directed to the N-HR region of gp41 model proteins.⁴⁴ 6-helix and 5-helix serve as good models for assessing the binding of the exogenously added C34 peptide by SEC–MALS. In the case of 6-helix, addition of a 5-fold excess of C34 results in the appearance of a small shoulder to the left of the major 6-helix peak that can be attributed to weak binding of C34 as a 1:1 complex (Figure 2A), presumably via displacement of the C-terminal C-HR

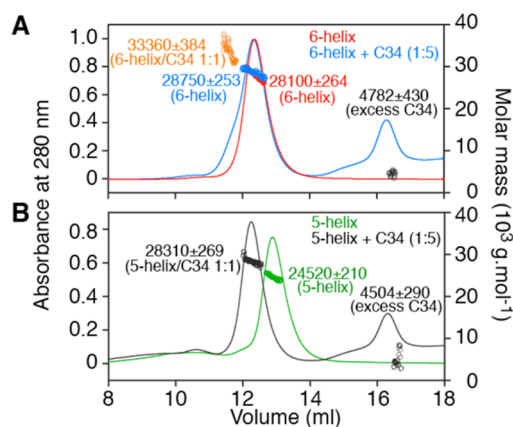


Figure 2. Molecular mass estimation by SEC–MALS under native conditions of 6-helix and 5-helix constructs in the presence or absence of excess C34 peptide. (A) Injection of 200 μ g of 6-helix alone (red) and with a 5-fold molar excess of C34 (blue). (B) Injection of 200 μ g of 5-helix alone (green) and with a 5-molar excess of C34 (black). Observed masses and compositions are indicated beside the peaks. Experiments were conducted in 10 mM Tris-HCl (pH 7.6) and 150 mM NaCl.

region (see below). In the case of 5-helix that lacks the last C-HR region, C34 binds with a 1:1 stoichiometry with a mass increase that clearly corresponds to the expected mass of C34 (Figure 2B).

Binding of C34 to the Native-like gp41 Mimetic, Core^S. Studies for assessing binding of C34 to gp41 constructs

containing the FPPR or MPER flanking region at the N- or C-terminus, respectively, of the core^S domain (Figure 1A) are not feasible because addition of detergent [e.g., dodecylphosphocholine (DPC)], which is essential to maintain the solubility of such longer constructs, dissociates the core^S trimer into monomers, even at pH 6, with no NMR-observable intramolecular contacts between the N-HR and CH-R regions of the monomer.^{49,57} Individual NH-R and CH-R peptides also associate with DPC.⁴⁹ Core^S and core^{SP}, on the other hand, are highly soluble under nearly physiological conditions, permitting a variety of analyses as described below in the absence of DPC.

SEC–MALS shows that addition of excess C34 to core^S results in the formation of a complex with a binding stoichiometry of one core^S trimer to two C34 peptides with no dissociation of the core^S trimer (Figure 3A). SEC–MALS of core^{SP}, which lacks the linker connecting the N-HR and C-HR regions, was used to assess whether binding of C34 occurs via displacement of the C-HR region. The appearance of a peak corresponding to the C38 peptide of core^{SP} upon addition of excess C34, coupled to the expected small reduction in the molecular weight of the “core^{SP}” peak, demonstrates that binding of C34 to core^{SP} is accompanied by displacement of C38. This result is confirmed by size-exclusion chromatography of core^{SP} bearing the Alexafluor 647 dye at the C-terminus of each C38 peptide that shows that addition of C34 results in the appearance of a C38-AL647 peak (Figure 3C,D).

Determination of the Apparent Binding Affinity of C34 to Core^S and Core^{SP}. Titration of C34 (0.05–0.1 mM) into 5–10 μ M core^S in the experimental buffer [10 mM Tris-HCl (pH 7.6) and 150 mM NaCl] at 25 °C did not yield a heat signature in ITC experiments conducted in a Microcal iTC200 instrument. This result resembles our earlier observation of no heat response upon titration of core^S with a neutralizing antibody that exhibits tight binding to core^S as revealed by native band-shift assays.⁴⁴ We therefore made use of C34 labeled with the Alexafluor 647 dye [C34-AL647 (Figure 1B)] to quantify the binding of C34 to core^S and core^{SP}.

Core^S was incubated with increasing concentrations of C34-AL647, and the resulting mixtures were analyzed by size-exclusion chromatography. As the relative absorbances at 609 and 650 nm differ depending on the intermolecular proximity of the dye molecules to one another (see Figure S1), the sum of the absorbances at these wavelengths was used to quantify the dye. The sum of peak areas at 609 and 650 nm for C34-AL647 free and in complex with core^S corresponds to the total concentration of C34-AL647 added to each sample, thereby validating this approach (Figure S1B). The sequential formation of 1:1 and 1:2 core^S–C34-AL647 complexes with increasing C34-AL647 concentrations, measured at three wavelengths, shows a decrease in absorbance at 280 nm of the peak with an elution volume of 13.7 mL corresponding to free core^S concomitant with the appearance of a 1:1 complex at \sim 12.5 mL, and subsequent appearance of a 1:2 complex (\sim 12.0 mL) (Figure S3). A similar experiment in which C34-AL647 was added to core^{SP} shows a less pronounced shift in the 280 nm absorbance corresponding to complex formation such that complexes with C34 are not readily distinguishable from core^{SP} based on their elution volumes (Figure S4).

Dissociation of the core^S trimer at ambient temperature in 10 mM Tris-HCl (pH 7.6) and 150 mM NaCl is expected to be <0.25 μ M based on estimating the mass as a function of the decreasing concentration (from 2 to 0.25 μ M) by composition

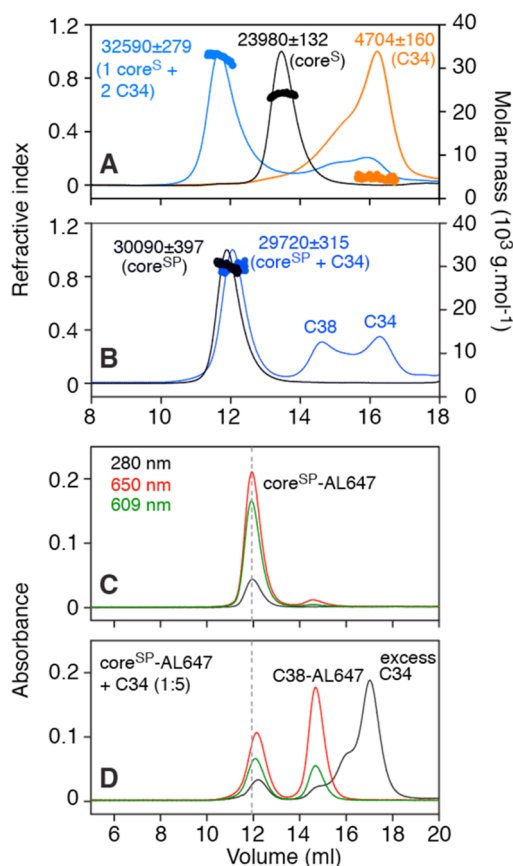
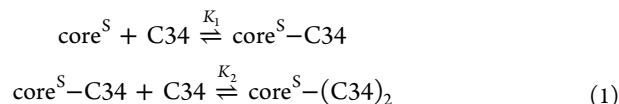


Figure 3. Size-exclusion chromatography elution profiles and mass analysis under native conditions of core^S, core^{SP}, and their complexes with C34. (A) SEC–MALS of the core^S trimer in the presence of a 5-fold molar excess of C34 (blue trace). Experimental masses and compositions are indicated beside the peaks. The peak for the complex is consistent with the binding of two C34 molecules to one core^S trimer. Control elution profiles (200 μg/100 μL injection) of core^S and C34 are colored black and orange, respectively. (B) SEC–MALS of core^{SP} (six-helix bundle assembled with individual N-HR and C-HR peptides) mixed with a 5-fold molar excess of C34 (blue trace). Observed peaks corresponding to C-HR peptide (C38, residues 625–662) and a complex of core^{SP} with C34 are consistent with displacement of C38 from core^{SP} by added excess C34. The elution profile and estimated mass of core^{SP} (control) are colored black. (C) Retention of core^{SP} labeled with AL647 matches the elution profile of unlabeled core^{SP} shown in panel B. (D) Displacement of AL647-labeled C38 by added C34 (5-fold molar excess) is consistent with data shown in panel B. Note that the relative extinction coefficients at 609 and 650 nm of AL647 differ depending on the proximity of the dyes to one another (elaborated in the text and Figure S1). Note also that two separate columns were used for SEC–MALS (panels A and B, flow rate of 0.5 mL/min) and absorbance measured at three wavelengths (panels C and D, flow rate of 0.7 mL/min); as a result, the retention volume for free C34 is slightly larger for the latter than the former. Experiments were conducted in 10 mM Tris-HCl (pH 7.6) and 150 mM NaCl.

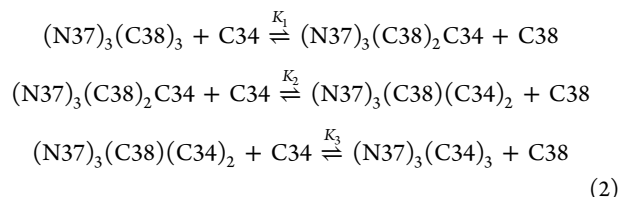
gradient–MALS analysis, the detection limit for core^S (data not shown). As both core^S and core^{SP} elute as stable trimers at an injected concentration of 2.33 μM with no discernible dissociation within the time scale of their elution and associated dilution by size-exclusion chromatography (~10-fold), even for core^{SP} that is assembled as peptides, we conclude that any exchange between components in the equilibrium mixture established prior to injection into the column is slow on the

time scale of the experiment and therefore no dilution factors or re-equilibration during the course of elution on the column needs be considered during the analysis of the equilibrium binding data.

Because the SEC–MALS and band-shift assays provide no evidence of the existence of a 1:3 core^S–(C34)₃ complex, the peak areas as a function of added C34 were analyzed in terms of formation of 1:1 and 1:2 complexes:



while for core^{SP}, (N37)₃(C38)₃, the data were analyzed in terms of three successive exchange reactions:



The summed peak areas at 609 and 650 nm are directly proportional to the concentration of bound C34 (cf. Figure S1), and thus, the measured peak area₆₀₉₊₆₅₀ for core^S is given by

$$\text{peak area}_{609+650} = S([\text{core}^S\text{-C34}] + 2[\text{core}^S\text{-(C34)}_2]) \quad (3)$$

and for core^{SP} by

$$\begin{aligned} \text{peak area}_{609+650} &= S\{[(\text{N37})_3(\text{C38})_2\text{C34}] \\ &\quad + 2[(\text{N37})_3(\text{C38})(\text{C34})_2] \\ &\quad + 3[(\text{N37})_3(\text{C34})_3]\} \end{aligned} \quad (4)$$

where *S* is a scale factor whose value is optimized during nonlinear least-squares minimization. In the case of core^S, we were also able to make use of the 280 nm data as the 1:1 and 1:2 complexes can be distinguished from free core^S (see Figure S3B). The combined area for the 1:1 and 1:2 peaks is then given by

$$\begin{aligned} \text{peak area}_{280}(1:1 + 1:2) \\ = S\{[\text{core}^S\text{-C34}] + \lambda[\text{core}^S\text{-(C34)}_2]\} \end{aligned} \quad (5)$$

where λ is the ratio of the extinction coefficients at 280 nm for the 1:2 to 1:1 complexes. λ has a value of 1.188 determined from the ε₂₈₀ values, calculated from amino acid sequence, of 66460 and 78950 M⁻¹ cm⁻¹ for the 1:1 and 1:2 complexes, respectively.⁵⁸ The resulting best fits to the experimental data are shown in panels A and B of Figure 4 for core^S and core^{SP}, respectively. The data show no evidence of any cooperativity: for core^S, K₁ = K₂ = (1.0 ± 0.1) × 10⁶ M⁻¹, and for core^{SP}, K₁ = K₂ = K₃ = 0.9 ± 0.1.

The value of 0.9 for the equilibrium constant for the exchange reaction of C34 with C38 in the case of core^{SP} is expected because one would predict that the affinity of C38 for the N-HR (N37)₃ trimer would be only minimally larger than for C34.

The value of 10⁶ M⁻¹ for the equilibrium association constant for the binding of C34 to core^S is also reasonable given that binding of C34 to core^S requires displacement of the

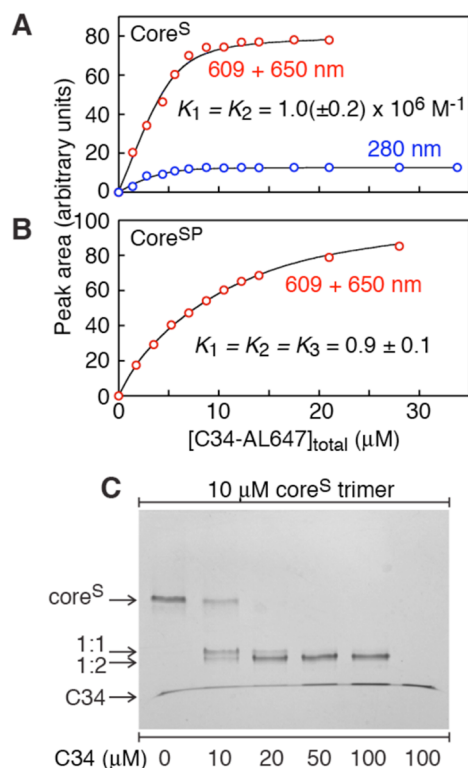


Figure 4. Characterization of the binding of C34 to core^S and core^{SP}. Fits (black lines) to the experimental data (red circles for the peak area at 609 + 650 nm, blue circles for the peak area at 280 nm) obtained by mixing 2.33 μM (A) core^S trimer and (B) core^{SP} (as a six-helix bundle) with increasing concentrations of C34-AL647 followed by size-exclusion chromatography and quantification (see Figures S3 and S4, respectively). For experimental details and data analysis, see the text. (C) Band shifts upon addition of increasing concentrations of C34 to a constant amount of core^S trimer analyzed by 20% homogeneous native-PAGE. Experiments were conducted in 10 mM Tris-HCl (pH 7.6) and 150 mM NaCl.

linked C28 C-HR from N34. The likely reason that a third molecule of C34 cannot bind to core^S is presumably due to the fact the resulting displaced C28 C-HRs are still covalently linked to the N-HR via a five-residue linker, and hence, the effective local concentration of C28 not in contact with the internal N-HR trimer, (N34)₃, is extremely high.

Native-PAGE of complexes also indicates that even at 3:1 and 3:2 core^S:C34 ratios (Figure 4C) a significant amount of complex comprising two C34 molecules bound to one core^S trimer is formed in a manner consistent with the binding data. The migration of free C34, which runs at the dye front, is retarded when it is in complex with core^S. In accordance, the band doublet observed in Figure 4C (lane 2) likely corresponds to 1:1 and 1:2 complexes of core^S with C34, with the 1:2 complex migrating slightly faster than the 1:1 complex.

Conformation of the C-HR of Core^S Displaced by C34.

To address the state of the displaced C28 C-HR of core^S upon C34 binding, we conducted EPR pulsed double electron-electron resonance (DEER) and CD measurements that provide distance (between nitroxide spin-labels) and secondary structure information, respectively.

Fully deuterated core^S constructs with nitroxide spin-labels added either at the N-terminus of the N-HR (construct N-Cys core^S) or at the C-terminus of the C-HR (construct C-Cys core^S) were employed. By significantly increasing the spin-label phase memory relaxation time, deuteration abolishes the dependence of the *P*(*r*) distance distribution on the length of the second echo period in the DEER experiment.⁵²

Addition of C34 to N-Cys core^S has a negligible effect on either the raw DEER dipolar evolution data (Figure 5A, left graph) or the derived *P*(*r*) distance distributions [obtained by Tikhonov regularization (Figure 5A, right graph)] that reflect the short intersubunit distances (<20 Å) between the nitroxide spin-labels in the trimer (see also Figure S5). One can therefore conclude that the N-HR helical trimer of core^S is essentially unperturbed upon binding C34 and concomitant displacement of the C28 C-HR.

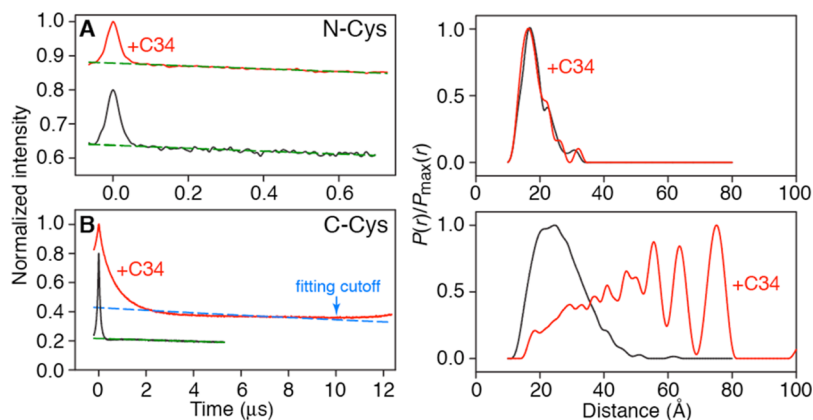


Figure 5. DEER EPR of N- and C-Cys nitroxide-labeled fully deuterated core^S constructs in the absence and presence of C34 peptide. Raw DEER data for N- and C-Cys MTSL deuterated core^S are shown in the left-hand graphs of panels A and B, respectively. Red and black curves represent data acquired with and without C34 peptide, respectively. Dashed dark green curves are the exponential background functions employed to separate the random intermolecular dipolar couplings from the desired intramolecular dipolar couplings. The results of the DeerAnalysis2013 Tikhonov Regularization fits⁵⁴ of the background-corrected data (see Figure S5) are shown in the right-hand graphs. It should be noted that the broad array of long (as much as 75 Å) spin-spin distances for C-Cys core^S in the presence of C34 makes background correction of the raw dipolar evolution data challenging and reduces the accuracy of the modeled *P*(*r*) distance distribution for this system (red curve in the left graph of panel B), such that relative peak intensities and peak positions can vary by as much as 30% and 2 Å, respectively, depending upon how the baseline subtraction is done. This, however, does not affect the conclusion that binding of two C34 molecules to core^S results in concomitant displacement of two C28 C-HRs from the internal N-HR trimer of core^S and that the displaced C28 C-HRs adopt a wide range of random-coil conformations.

In the case of the C-Cys core^S, however, a very large increase in the average distance between electron spins upon addition of C34 is immediately apparent from inspection of the raw DEER dipolar evolution data (Figure 5B, left graph), ranging from 20 to 75 Å (red curve in the right graph of Figure 5B), indicating that the displaced C28 C-HRs attached to the N34 N-HR by a five-residue linker adopt a wide variety of presumably random-coil conformations.

CD spectra of C34, and core^S and core^{SP} in the absence and presence of C34, are shown in Figure 6. Binding of C34 to the

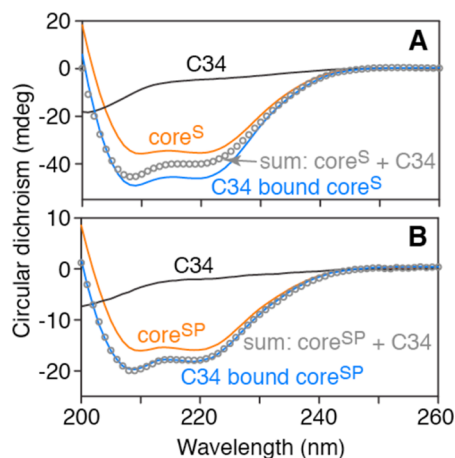


Figure 6. CD analysis of core^S and core^{SP} in the absence and presence of a 5-fold molar excess of C34. CD spectra of (A) core^S (7 μM as a trimer) and (B) core^{SP} (2.5 μM as a trimer, N-HR and C-HR peptides calculated as 1 unit) in the absence (orange line) and presence (blue line) of a 5-fold excess of C34. C34 alone (black line) shows no helical signature. The gray circles are the sums of the CD spectra of core^S or core^{SP} and C34.

N-HR (N37)₃ trimer of core^{SP} with concomitant dissociation of C38 results in no change in helicity (Figure 6B), as expected because the number of residues in contact with the N-HR (N37)₃ trimer is predicted to be similar for C34 and C38^{13,14} and free C38 is a random coil. In the case of core^S, however, binding of two C34 molecules together with displacement of two C28 C-HR chains results in an ~18% increase in helicity (Figure 6A), corresponding to an additional 30 residues of the trimer in a helical conformation (6 × 3 from the N34 N-HR trimer and 2 × 6 from two molecules of C34 bound).

T20 Does Not Bind to Core^S. The T20 peptide (also known as Enfuvirtide or Fuzeon) comprising residues 638–673 of gp41 is a drug in clinical use as an inhibitor of HIV-1 fusion.^{59–61} Although T20 overlaps a major part of the C34 sequence, it lacks residues 628–637 of C34 at its N-terminus but extends 11 residues into the MPER domain at its C-terminus (Figure 1). The partial sequence overlap of T20 with C34 had suggested a similar mode of interaction with gp41 analogues. However, we were unable to detect binding of T20 to core^S (Figure 7A) or 5-helix (Figure 7B) under conditions where binding of C34 is clearly evident (Figures 4C and 7B), suggesting a different mode of action with regard to inhibition of HIV-1 fusion.⁶² This is supported by previous findings that binding of T20 to 5-helix is 6 orders of magnitude weaker than that of C37, a peptide similar to C34 but with a three-residue N-terminal extension,⁶³ and that enhanced membrane interactions of T20 via the C-terminal WNWF sequence are an essential determinant of T20 potency.^{64–66} As T20 could not

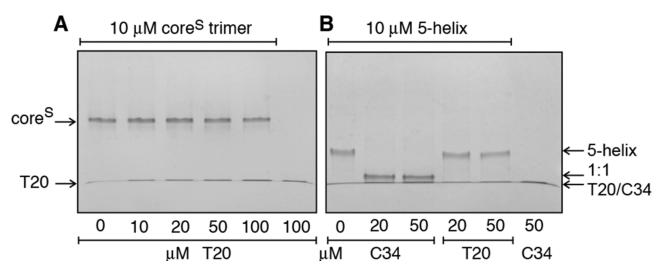


Figure 7. Assessment of binding of the T20 peptide to (A) core^S and (B) 5-helix by native-PAGE. Binding of C34 to 5-helix is shown in panel B as a positive control with a 1:1 stoichiometry of binding (see Figure 2).

be fractionated on a Superdex-75 column in the current experimental buffer because of nonspecific interactions with the column matrix, similar analysis as described for the displacement of labeled C38-AL647 from core^{SP}-AL647 by C34 (Figure 3C,D) could not be conducted by adding T20 to the core^{SP}-AL647 trimer.

CONCLUDING REMARKS

Using a variety of biophysical techniques, we have shown that the C34 HIV-1 fusion inhibitory peptide can bind not only to prehairpin intermediate mimetics of gp41 in which the N-HR trimer is fully solvent-exposed but also to the fusogenic/postfusogenic six-helix bundle conformation. In contrast to monoclonal antibodies targeted against the N-HR trimer that are also capable of binding to six-helix bundle mimetics via a small exposed hydrophobic pocket formed by the N-HR helices,⁴⁴ binding of C34 occurs via complete displacement of the external C-HR helices. These results may relate to the conclusions of Markosyan et al.¹⁷ that the time window of C34 fusion inhibitory activity can extend from the point at which the prehairpin intermediate of gp41 becomes accessible through the formation of late prebundle intermediates and labile pore formation, but not after irreversible formation of the six-helix bundle required for robust pore formation and enlargement. The core^S model may represent a conformational state in trimer stability among a continuum of states similar to a late prebundle because core^S permits displacement of the C-HR by C34 and thus provides a basis for exploring the binding of C34 in the absence of DPC and possibly of the binding of T20 to longer gp41 mimetics that span either the FPPR or MPER regions, or both, in membrane-mimicking environments. Additionally, the method described here for monitoring binding to the six-helix bundle of the gp41 ectodomain by displacement of dye labeled C38 C-HR may prove to be useful for facile screening of compounds with properties similar to those of C34.

ASSOCIATED CONTENT

Supporting Information

The Supporting Information is available free of charge on the ACS Publications website at DOI: 10.1021/acs.biochem.5b01021.

Five supplementary figures pertaining to the properties of the AL647 dye, thermal melting, additional size-exclusion chromatography profiles, and EPR data (PDF)

AUTHOR INFORMATION

Corresponding Authors

*Laboratory of Chemical Physics, National Institute of Diabetes and Digestive and Kidney Diseases, National Institutes of Health, Bethesda, MD 20892-0520. E-mail: johnl@niddk.nih.gov.

*E-mail: mariusc@mail.nih.gov.

Funding

This research was supported by the Intramural Research Program of the National Institute of Diabetes and Digestive and Kidney Diseases, National Institutes of Health, and the Intramural AIDS-Targeted Program of the Office of the Director, National Institutes of Health (to G.M.C.).

Notes

The authors declare no competing financial interest.

ACKNOWLEDGMENTS

We thank Jane M. Sayer, Julien Roche, and Ad Bax for helpful discussions and Annie Aniana for technical assistance. T20 was obtained through the NIH AIDS Research and Reference Reagent Program, Division of AIDS, National Institute of Allergy and Infectious Diseases, National Institutes of Health. We acknowledge use of the National Institute of Diabetes and Digestive and Kidney Diseases Advanced Mass Spectrometry Core Facility.

REFERENCES

(1) Freed, E. O., and Martin, M. A. (1995) The role of human immunodeficiency virus type 1 envelope glycoproteins in virus infection. *J. Biol. Chem.* 270, 23883–23886.

(2) Moore, J. P., Trkola, A., and Dragic, T. (1997) Co-receptors for HIV-1 entry. *Curr. Opin. Immunol.* 9, 551–562.

(3) Berger, E. A., Murphy, P. M., and Farber, J. M. (1999) Chemokine receptors as HIV-1 coreceptors: roles in viral entry, tropism, and disease. *Annu. Rev. Immunol.* 17, 657–700.

(4) Eckert, D. M., and Kim, P. S. (2001) Mechanisms of viral membrane fusion and its inhibition. *Annu. Rev. Biochem.* 70, 777–810.

(5) Gallo, S. A., Finnegan, C. M., Viard, M., Raviv, Y., Dimitrov, A., Rawat, S. S., Puri, A., Durell, S., and Blumenthal, R. (2003) The HIV Env-mediated fusion reaction. *Biochim. Biophys. Acta, Biomembr.* 1614, 36–50.

(6) Miyachi, K., Kim, Y., Latinovic, O., Morozov, V., and Melikyan, G. B. (2009) HIV enters cells via endocytosis and dynamin-dependent fusion with endosomes. *Cell* 137, 433–444.

(7) Blumenthal, R., Durell, S., and Viard, M. (2012) HIV entry and envelope glycoprotein-mediated fusion. *J. Biol. Chem.* 287, 40841–40849.

(8) Julien, J. P., Cupo, A., Sok, D., Stanfield, R. L., Lyumkis, D., Deller, M. C., Klasse, P. J., Burton, D. R., Sanders, R. W., Moore, J. P., Ward, A. B., and Wilson, I. A. (2013) Crystal structure of a soluble cleaved HIV-1 envelope trimer. *Science* 342, 1477–1483.

(9) Lyumkis, D., Julien, J. P., de Val, N., Cupo, A., Potter, C. S., Klasse, P. J., Burton, D. R., Sanders, R. W., Moore, J. P., Carragher, B., Wilson, I. A., and Ward, A. B. (2013) Cryo-EM structure of a fully glycosylated soluble cleaved HIV-1 envelope trimer. *Science* 342, 1484–1490.

(10) Furuta, R. A., Wild, C. T., Weng, Y., and Weiss, C. D. (1998) Capture of an early fusion-active conformation of HIV-1 gp41. *Nat. Struct. Biol.* 5, 276–279.

(11) Chan, D. C., and Kim, P. S. (1998) HIV entry and its inhibition. *Cell* 93, 681–684.

(12) Root, M. J., and Steger, H. K. (2004) HIV-1 gp41 as a target for viral entry inhibition. *Curr. Pharm. Des.* 10, 1805–1825.

(13) Chan, D. C., Fass, D., Berger, J. M., and Kim, P. S. (1997) Core structure of gp41 from the HIV envelope glycoprotein. *Cell* 89, 263–273.

(14) Weissenhorn, W., Dessen, A., Harrison, S. C., Skehel, J. J., and Wiley, D. C. (1997) Atomic structure of the ectodomain from HIV-1 gp41. *Nature* 387, 426–430.

(15) Caffrey, M., Cai, M., Kaufman, J., Stahl, S. J., Wingfield, P. T., Covell, D. G., Gronenborn, A. M., and Clore, G. M. (1998) Three-dimensional solution structure of the 44 kDa ectodomain of SIV gp41. *EMBO J.* 17, 4572–4584.

(16) Tan, K., Liu, J., Wang, J., Shen, S., and Lu, M. (1997) Atomic structure of a thermostable subdomain of HIV-1 gp41. *Proc. Natl. Acad. Sci. U. S. A.* 94, 12303–12308.

(17) Markosyan, R. M., Cohen, F. S., and Melikyan, G. B. (2003) HIV-1 envelope proteins complete their folding into six-helix bundles immediately after fusion pore formation. *Mol. Biol. Cell* 14, 926–938.

(18) Melikyan, G. B. (2008) Common principles and intermediates of viral protein-mediated fusion: the HIV-1 paradigm. *Retrovirology* 5, 111.

(19) Wild, C. T., Shugars, D. C., Greenwell, T. K., McDanal, C. B., and Matthews, T. J. (1994) Peptides corresponding to a predictive alpha-helical domain of human immunodeficiency virus type 1 gp41 are potent inhibitors of virus infection. *Proc. Natl. Acad. Sci. U. S. A.* 91, 9770–9774.

(20) Louis, J. M., Bewley, C. A., and Clore, G. M. (2001) Design and properties of N_{CCG}-gp41, a chimeric gp41 molecule with nanomolar HIV fusion inhibitory activity. *J. Biol. Chem.* 276, 29485–29489.

(21) Root, M. J., Kay, M. S., and Kim, P. S. (2001) Protein design of an HIV-1 entry inhibitor. *Science* 291, 884–888.

(22) Louis, J. M., Nesheiwat, I., Chang, L., Clore, G. M., and Bewley, C. A. (2003) Covalent trimers of the internal N-terminal trimeric coiled-coil of gp41 and antibodies directed against them are potent inhibitors of HIV envelope-mediated cell fusion. *J. Biol. Chem.* 278, 20278–20285.

(23) Kilgore, N. R., Salzwedel, K., Reddick, M., Allaway, G. P., and Wild, C. T. (2003) Direct evidence that C-peptide inhibitors of human immunodeficiency virus type 1 entry bind to the gp41 N-helical domain in receptor-activated viral envelope. *J. Virol.* 77, 7669–7672.

(24) Root, M. J., and Hamer, D. H. (2003) Targeting therapeutics to an exposed and conserved binding element of the HIV-1 fusion protein. *Proc. Natl. Acad. Sci. U. S. A.* 100, 5016–5021.

(25) Steger, H. K., and Root, M. J. (2006) Kinetic dependence to HIV-1 entry inhibition. *J. Biol. Chem.* 281, 25813–25821.

(26) Welch, B. D., Francis, J. N., Redman, J. S., Paul, S., Weinstock, M. T., Reeves, J. D., Lie, Y. S., Whitby, F. G., Eckert, D. M., Hill, C. P., Root, M. J., and Kay, M. S. (2010) Design of a potent D-peptide HIV-1 entry inhibitor with a strong barrier to resistance. *J. Virol.* 84, 11235–11244.

(27) Chan, D. C., Chutkowski, C. T., and Kim, P. S. (1998) Evidence that a prominent cavity in the coiled coil of HIV type 1 gp41 is an attractive drug target 2. *Proc. Natl. Acad. Sci. U. S. A.* 95, 15613–15617.

(28) Golding, H., Zaitseva, M., de Rosny, E., King, L. R., Manischewitz, J., Sidorov, I., Gorny, M. K., Zolla-Pazner, S., Dimitrov, D. S., and Weiss, C. D. (2002) Dissection of human immunodeficiency virus type 1 entry with neutralizing antibodies to gp41 fusion intermediates. *J. Virol.* 76, 6780–6790.

(29) Louis, J. M., Bewley, C. A., Gustchina, E., Aniana, A., and Marius Clore, G. (2005) Characterization and HIV-1 fusion inhibitory properties of monoclonal Fabs obtained from a human non-immune phage library selected against diverse epitopes of the ectodomain of HIV-1 gp41. *J. Mol. Biol.* 353, 945–951.

(30) Gustchina, E., Louis, J. M., Lam, S. N., Bewley, C. A., and Clore, G. M. (2007) A monoclonal Fab derived from a human nonimmune phage library reveals a new epitope on gp41 and neutralizes diverse human immunodeficiency virus type 1 strains. *J. Virol.* 81, 12946–12953.

(31) Gustchina, E., Louis, J. M., Frisch, C., Ylera, F., Lechner, A., Bewley, C. A., and Clore, G. M. (2009) Affinity maturation by targeted diversification of the CDR-H2 loop of a monoclonal Fab derived from

a synthetic naive human antibody library and directed against the internal trimeric coiled-coil of gp41 yields a set of Fabs with improved HIV-1 neutralization potency and breadth. *Virology* 393, 112–119.

(32) Gustchina, E., Li, M., Louis, J. M., Anderson, D. E., Lloyd, J., Frisch, C., Bewley, C. A., Gustchina, A., Wlodawer, A., and Clore, G. M. (2010) Structural basis of HIV-1 neutralization by affinity matured Fabs directed against the internal trimeric coiled-coil of gp41. *PLoS Pathog.* 6, e1001182.

(33) Gustchina, E., Li, M., Ghirlando, R., Schuck, P., Louis, J. M., Pierson, J., Rao, P., Subramaniam, S., Gustchina, A., Clore, G. M., and Wlodawer, A. (2013) Complexes of neutralizing and non-neutralizing affinity matured fabs with a mimetic of the internal trimeric coiled-coil of HIV-1 gp41. *PLoS One* 8, e78187.

(34) Miller, M. D., Geleziunas, R., Bianchi, E., Lennard, S., Hrin, R., Zhang, H., Lu, M., An, Z., Ingallinella, P., Finotto, M., Mattu, M., Finnefrock, A. C., Bramhill, D., Cook, J., Eckert, D. M., Hampton, R., Patel, M., Jarantow, S., Joyce, J., Ciliberto, G., Cortese, R., Lu, P., Strohl, W., Schleif, W., McElhaugh, M., Lane, S., Lloyd, C., Lowe, D., Osbourn, J., Vaughan, T., Emini, E., Barbato, G., Kim, P. S., Hazuda, D. J., Shiver, J. W., and Pessi, A. (2005) A human monoclonal antibody neutralizes diverse HIV-1 isolates by binding a critical gp41 epitope. *Proc. Natl. Acad. Sci. U. S. A.* 102, 14759–14764.

(35) Luftig, M. A., Mattu, M., Di Giovine, P., Geleziunas, R., Hrin, R., Barbato, G., Bianchi, E., Miller, M. D., Pessi, A., and Carfi, A. (2006) Structural basis for HIV-1 neutralization by a gp41 fusion intermediate-directed antibody. *Nat. Struct. Mol. Biol.* 13, 740–747.

(36) Nelson, J. D., Kinkead, H., Brunel, F. M., Leaman, D., Jensen, R., Louis, J. M., Maruyama, T., Bewley, C. A., Bowdish, K., Clore, G. M., Dawson, P. E., Frederickson, S., Mage, R. G., Richman, D. D., Burton, D. R., and Zwick, M. B. (2008) Antibody elicited against the gp41 N-heptad repeat (NHR) coiled-coil can neutralize HIV-1 with modest potency but non-neutralizing antibodies also bind to NHR mimetics. *Virology* 377, 170–183.

(37) Choudhry, V., Zhang, M. Y., Sidorov, I. A., Louis, J. M., Harris, I., Dimitrov, A. S., Bouma, P., Cham, F., Choudhary, A., Rybak, S. M., Fouts, T., Montefiori, D. C., Broder, C. C., Quinnan, G. V., Jr., and Dimitrov, D. S. (2007) Cross-reactive HIV-1 neutralizing monoclonal antibodies selected by screening of an immune human phage library against an envelope glycoprotein (gp140) isolated from a patient (R2) with broadly HIV-1 neutralizing antibodies. *Virology* 363, 79–90.

(38) Zhang, M. Y., Vu, B. K., Choudhary, A., Lu, H., Humbert, M., Ong, H., Alam, M., Ruprecht, R. M., Quinnan, G., Jiang, S., Montefiori, D. C., Mascola, J. R., Broder, C. C., Haynes, B. F., and Dimitrov, D. S. (2008) Cross-reactive human immunodeficiency virus type 1-neutralizing human monoclonal antibody that recognizes a novel conformational epitope on gp41 and lacks reactivity against self-antigens. *J. Virol.* 82, 6869–6879.

(39) Eckert, D. M., Shi, Y., Kim, S., Welch, B. D., Kang, E., Poff, E. S., and Kay, M. S. (2008) Characterization of the steric defense of the HIV-1 gp41 N-trimer region. *Protein Sci.* 17, 2091–2100.

(40) Sabin, C., Corti, D., Buzon, V., Seaman, M. S., Lutje Hulsik, D., Hinz, A., Vanzetta, F., Agatic, G., Silacci, C., Mainetti, L., Scarlatti, G., Sallusto, F., Weiss, R., Lanzavecchia, A., and Weissenhorn, W. (2010) Crystal structure and size-dependent neutralization properties of HK20, a human monoclonal antibody binding to the highly conserved heptad repeat 1 of gp41. *PLoS Pathog.* 6, e1001195.

(41) Lai, R. P., Hock, M., Radzimanowski, J., Tonks, P., Hulsik, D. L., Effantin, G., Seilly, D. J., Dreja, H., Kliche, A., Wagner, R., Barnett, S. W., Tumba, N., Morris, L., LaBranche, C. C., Montefiori, D. C., Seaman, M. S., Heeney, J. L., and Weissenhorn, W. (2014) A fusion intermediate gp41 immunogen elicits neutralizing antibodies to HIV-1. *J. Biol. Chem.* 289, 29912–29926.

(42) Bewley, C. A., Louis, J. M., Ghirlando, R., and Clore, G. M. (2002) Design of a novel peptide inhibitor of HIV fusion that disrupts the internal trimeric coiled-coil of gp41. *J. Biol. Chem.* 277, 14238–14245.

(43) Gustchina, E., Bewley, C. A., and Clore, G. M. (2008) Sequestering of the prehairpin intermediate of gp41 by peptide N36Mut(e,g) potentiates the human immunodeficiency virus type 1

neutralizing activity of monoclonal antibodies directed against the N-terminal helical repeat of gp41. *J. Virol.* 82, 10032–10041.

(44) Louis, J. M., Aniana, A., Lohith, K., Sayer, J. M., Roche, J., Bewley, C. A., and Clore, G. M. (2014) Binding of HIV-1 gp41-directed neutralizing and non-neutralizing fragment antibody binding domain (Fab) and single chain variable fragment (ScFv) antibodies to the ectodomain of gp41 in the pre-hairpin and six-helix bundle conformations. *PLoS One* 9, e104683.

(45) Deng, Y., Zheng, Q., Ketas, T. J., Moore, J. P., and Lu, M. (2007) Protein design of a bacterially expressed HIV-1 gp41 fusion inhibitor. *Biochemistry* 46, 4360–4369.

(46) Chong, H., Yao, X., Sun, J., Qiu, Z., Zhang, M., Waltersperger, S., Wang, M., Cui, S., and He, Y. (2012) The M-T hook structure is critical for design of HIV-1 fusion inhibitors. *J. Biol. Chem.* 287, 34558–34568.

(47) He, Y., Liu, S., Jing, W., Lu, H., Cai, D., Chin, D. J., Debnath, A. K., Kirchoff, F., and Jiang, S. (2007) Conserved residue Lys574 in the cavity of HIV-1 Gp41 coiled-coil domain is critical for six-helix bundle stability and virus entry. *J. Biol. Chem.* 282, 25631–25639.

(48) Gustchina, E., Hummer, G., Bewley, C. A., and Clore, G. M. (2005) Differential inhibition of HIV-1 and SIV envelope-mediated cell fusion by C34 peptides derived from the C-terminal heptad repeat of gp41 from diverse strains of HIV-1, HIV-2, and SIV. *J. Med. Chem.* 48, 3036–3044.

(49) Roche, J., Louis, J. M., Aniana, A., Ghirlando, R., and Bax, A. (2015) Complete dissociation of the HIV-1 gp41 ectodomain and membrane proximal regions upon phospholipid binding. *J. Biomol. NMR* 61, 235–248.

(50) Bohm, G., Muhr, R., and Jaenicke, R. (1992) Quantitative analysis of protein far UV circular dichroism spectra by neural networks. *Protein Eng., Des. Sel.* 5, 191–195.

(51) Chance, E. M. C., Jones, I. P., and Kirby, C. R. (1979) *FACSIMILE: A computer program for flow and chemistry simulation and general initial value problems.* Atomic Energy Research Establishment Report R8775, Her Majesty's Stationery Office, London.

(52) Baber, J. L., Louis, J. M., and Clore, G. M. (2015) Dependence of distance distributions derived from double electron-electron resonance pulsed EPR spectroscopy on pulse-sequence time. *Angew. Chem., Int. Ed.* 54, 5336–5339.

(53) Pannier, M., Veit, S., Godt, A., Jeschke, G., and Spiess, H. W. (2000) Dead-time free measurement of dipole-dipole interactions between electron spins. *J. Magn. Reson.* 142, 331–340.

(54) Jeschke, G., Chechik, V., Ionita, P., Godt, A., Zimmermann, H., Banham, J., Timmel, C. R., Hilger, D., and Jung, H. (2006) DeerAnalysis2006 - a comprehensive software package for analyzing pulsed ELDOR data. *Appl. Magn. Reson.* 30, 473–498.

(55) von Hagens, T., Polyhach, Y., Sajid, M., Godt, A., and Jeschke, G. (2013) Suppression of ghost distances in multiple-spin double electron-electron resonance. *Phys. Chem. Chem. Phys.* 15, 5854–5866.

(56) Dai, Z., Tao, Y., Liu, N., Brenowitz, M. D., Girvin, M. E., and Lai, J. R. (2015) Conditional trimerization and lytic activity of HIV-1 gp41 variants containing the membrane-associated segments. *Biochemistry* 54, 1589–1599.

(57) Roche, J., Louis, J. M., Grishaev, A., Ying, J., and Bax, A. (2014) Dissociation of the trimeric gp41 ectodomain at the lipid-water interface suggests an active role in HIV-1 Env-mediated membrane fusion. *Proc. Natl. Acad. Sci. U. S. A.* 111, 3425–3430.

(58) Anthis, N. J., and Clore, G. M. (2013) Sequence-specific determination of protein and peptide concentrations by absorbance at 205 nm. *Protein Sci.* 22, 851–858.

(59) Lalezari, J. P., Henry, K., O'Hearn, M., Montaner, J. S., Piliero, P. J., Trottier, B., Walmsley, S., Cohen, C., Kuritzkes, D. R., Eron, J. J., Jr., Chung, J., DeMasi, R., Donatucci, L., Drobnes, C., Delehanty, J., and Salgo, M. (2003) Enfuvirtide, an HIV-1 fusion inhibitor, for drug-resistant HIV infection in North and South America. *N. Engl. J. Med.* 348, 2175–2185.

(60) Lazzarin, A., Clotet, B., Cooper, D., Reynes, J., Arasteh, K., Nelson, M., Katlama, C., Stellbrink, H. J., Delfraissy, J. F., Lange, J., Huson, L., DeMasi, R., Wat, C., Delehanty, J., Drobnes, C., and Salgo,

M. (2003) Efficacy of enfuvirtide in patients infected with drug-resistant HIV-1 in Europe and Australia. *N. Engl. J. Med.* 348, 2186–2195.

(61) Matthews, T., Salgo, M., Greenberg, M., Chung, J., DeMasi, R., and Bolognesi, D. (2004) Enfuvirtide: the first therapy to inhibit the entry of HIV-1 into host CD4 lymphocytes. *Nat. Rev. Drug Discovery* 3, 215–225.

(62) Liu, S., Lu, H., Niu, J., Xu, Y., Wu, S., and Jiang, S. (2005) Different from the HIV fusion inhibitor C34, the anti-HIV drug Fuzeon (T-20) inhibits HIV-1 entry by targeting multiple sites in gp41 and gp120. *J. Biol. Chem.* 280, 11259–11273.

(63) Champagne, K., Shishido, A., and Root, M. J. (2009) Interactions of HIV-1 inhibitory peptide T20 with the gp41 N-HR coiled coil. *J. Biol. Chem.* 284, 3619–3627.

(64) Peisajovich, S. G., Gallo, S. A., Blumenthal, R., and Shai, Y. (2003) C-terminal octylation rescues an inactive T20 mutant: implications for the mechanism of HIV/SIMIAN immunodeficiency virus-induced membrane fusion. *J. Biol. Chem.* 278, 21012–21017.

(65) Wexler-Cohen, Y., and Shai, Y. (2007) Demonstrating the C-terminal boundary of the HIV 1 fusion conformation in a dynamic ongoing fusion process and implication for fusion inhibition. *FASEB J.* 21, 3677–3684.

(66) Ashkenazi, A., Wexler-Cohen, Y., and Shai, Y. (2011) Multifaceted action of Fuzeon as virus-cell membrane fusion inhibitor. *Biochim. Biophys. Acta, Biomembr.* 1808, 2352–2358.